Analysis of Cliff Effects and Thermal Hydraulic Instabilities in the PLANDTL-2 Sodium Experiment Transient Tests

Sébastien Renaudière de Vaux, Simon Li, Toshiki Ezure, Masaaki Tanaka

NURETH-21 21st International Topical Meeting on Nuclear Reactor Thermal Hydraulics
August 31 (Sun) - September 5 (Fri), 2025
BEXCO · Busan, Korea
www.nureth-21.org

Analysis of Cliff Effects and Thermal Hydraulic Instabilities in the PLANDTL-2 Sodium Experiment Transient Tests

Sébastien Renaudière de Vaux, Simon Li
CEA Cadarache (French Atomic Energy Commission) 13108 Saint-Paul-lez-Durance, France
sebastien.renaudieredevaux@cea.fr, simon.li@cea.fr

Toshiki Ezure, Masaaki Tanaka
Japan Atomic Energy Agency (JAEA) of Oarai, Japan
ezure.toshiki@jaea.go.jp, tanaka.masaaki@jaea.go.jp

ABSTRACT

Separate Effect Tests (SET) and Integral Effect Tests (IET) are commonly used in support of reactor designs, both to analyze physical phenomena and to validate simulation codes. In the framework of the Franco-Japanese collaboration on Research and Development for Sodium Fast Reactors (SFR) thermal hydraulics, transient tests were performed in the IET named PLANDTL-2 test facility in Japan. This IET's instrumented test section is composed of an electrically heated core and a hot pool with a Dipped Heat Exchanger (DHX). The Intermediate Heat Exchanger (IHX) and the Electro-Magnetic Pump (EMP) are located in a deported primary loop. Studied transients consist in transition from forced to natural convection, in the hot pool and in the primary circuit, under various decay heat removal operations using the DHX. It was observed that in the long term, a cliff effect occurs, meaning that the apparent steady natural convection is perturbed if a threshold is reached. Instabilities and flowrate oscillations from positive to negative values in the primary loop are observed after a period of smooth natural circulation. The unstable behavior results from the competition between IHX and DHX cooling, the latter leading to an increase in thermal stratification in the hot pool. This paper aims to analyze this phenomenon, bring a comprehensive criterion for the onset of unstable behaviors and give some general guidelines to avoid such effects for accidental transient management.

KEYWORDS
Sodium Fast Reactor, PLANDTL-2, Natural Convection, Instabilities, Integral Effect Test

1. INTRODUCTION

Ensuring effective heat removal from a nuclear reactor core during unexpected events is a critical safety consideration. The primary objective is to prevent damage to the core and its supporting structures by maintaining adequate cooling. Passive cooling systems have emerged as a promising solution, as they operate without external power sources or human intervention, relying instead on natural circulation. This approach has been integrated into various Sodium-cooled Fast Reactor (SFR) designs. One passive decay heat removal strategy involves the use of a Dipped Heat eXchanger (DHX) immersed in the hot pool as part of the Decay Heat Removal System (DHRS) [1, 2].

Despite their potential, significant challenges remain in the design and development of these systems, particularly for liquid metal reactors. Computational Fluid Dynamics (CFD) models, while essential for understanding thermal and flow phenomena, require extensive validation based on experimental data [3]. Thermal stratification, a critical phenomenon in pool-type reactors, remains an active area of research [4, 5], particularly due to its potential to alter flowrates [6, 7, 8]. During a transition from forced to natural circulation, such as during a primary pump trip, system-scale codes often fail to capture these dynamics accurately, necessitating multiscale simulations [6, 9]. Additionally, thermal stratification can lead to large temperature fluctuations [10], and in extreme cases, hinder the establishment of natural

circulation. Facilities like STELLA-2 [11, 12] and CLEAR-S [4] have provided valuable insights into strong stratification behaviors through experiments and CFD studies. Strategies for numerical investigations have ranged from detailed CFD simulations to emerging approaches, such as 1D modeling of stratification [6, 7, 8], offering computationally efficient alternatives.

Experimental findings from the previous configuration of the PLANDTL (Plant Dynamics Test Loop) facility highlight the significant role of Inter-Wrapper Flow (IWF) in enhancing core cooling through 3D fluid motion [13] (including cross and reverse flow between the assemblies). Stability remains a critical concern for passive systems, as various types of instabilities ranging from two-phase flow dynamics [14, 15] to single-phase natural circulation oscillations [16, 17] can compromise decay heat removal. Most studies on accidental transients focus on short-term [4] or medium-term [5, 11] phases, leaving long-term behavior ($>$ 600 minutes) largely unexplored except in select cases [8].

The PLANDTL-2 facility is an Integral Effect Test (IET) sodium loop designed to study Decay Heat Removal Systems (DHRS) in SFR concepts [18, 19, 20]. The geometry and experimental conditions are carefully designed to provide quantitative and qualitative insights into the reactor's actual behavior, such as the ASTRID concept [21]. In the experiments discussed here, the core was initially cooled by forced convection through the primary circuit. Then, the primary circuit flow transited to natural circulation, and the decay heat is removed inside the reactor vessel using a DHX. Moreover, shutdown procedures of the secondary circuit, and startup procedures of DHRS were varied as experimental parameters resulting in eight test cases. In addition, these tests were carried out over several hours. It allowed to identify long-term phenomena such as three dimensional effects or thermal stratification. Such effects prevent the use of 0D (homogeneous) models of system-scale codes such as CATHARE.

This study investigates the onset of instability and flow reversals driven by strong thermal stratification in a sodium pool. We identify cliff effects, i.e. flow reversals, occurring 100–200 minutes into a transient and demonstrate that intuitive strategies to rapidly cool the hot pool may induce unstable behaviors. Counterintuitively, the cooling rate of safety systems should be moderate during the initial phase of a transient to avoid such instabilities. We first describe the loop geometry and the transient scenarios in Section 2. Section 3 presents the experimental findings on heat transfer and flow dynamics. Section 4 provides a detailed discussion of the results, along with proposed guidelines. Finally, Section 5 concludes with key insights both for future campaigns and for reactor design and broader perspectives on this work.

2. LOOP GEOMETRY AND TRANSIENT SCENARIOS

2.1. PLANDTL-2 Facility

The PLANDTL-2 test-section is shown in Figure 1. First, the core behavior is modeled using electrically heated pins housed within the lower section of a cylindrical structure. The core consists of 30 heated assemblies, surrounded by a ring of unheated assemblies positioned at its periphery. A non-heated channels is at the center of the core. The inlet of the core is separated in two distinct inlet plenums. One feeds the heated pins, while the second one feeds the peripheral unheated pins. The core diameter is about 1 m.

Next, the hot pool is located above the core. It contains the Upper Internal Structure (UIS), two hot legs (HL) in upper configuration and the DHX. The DHX is part of the DHRS, and its location is as indicated in Figure 1. The HLs are opposed to each other. The HL are linked to a deported Intermediate Heat eXchanger (IHX). Four dummy cold legs (CL) are also inserted in order to mimic the flow-structure interaction that would occur in a pool design. The hot pool diameter is about 2 m. The test-section is fully instrumented by several flowrate measurements, temperature measurements with thermocouples (TCs) and several TC-trees are dipped inside the pool.

The global layout of the system is shown in Figure 2. The arrows indicate the flow direction in nominal conditions. In normal operation, the Electro-Magnetic Pumps (EMPs) enable the flow circulation throughout the primary and secondary circuits. In the natural circulation transients considered here, all EMPs are shut down shortly after the beginning of the transient. The heat is transferred from the

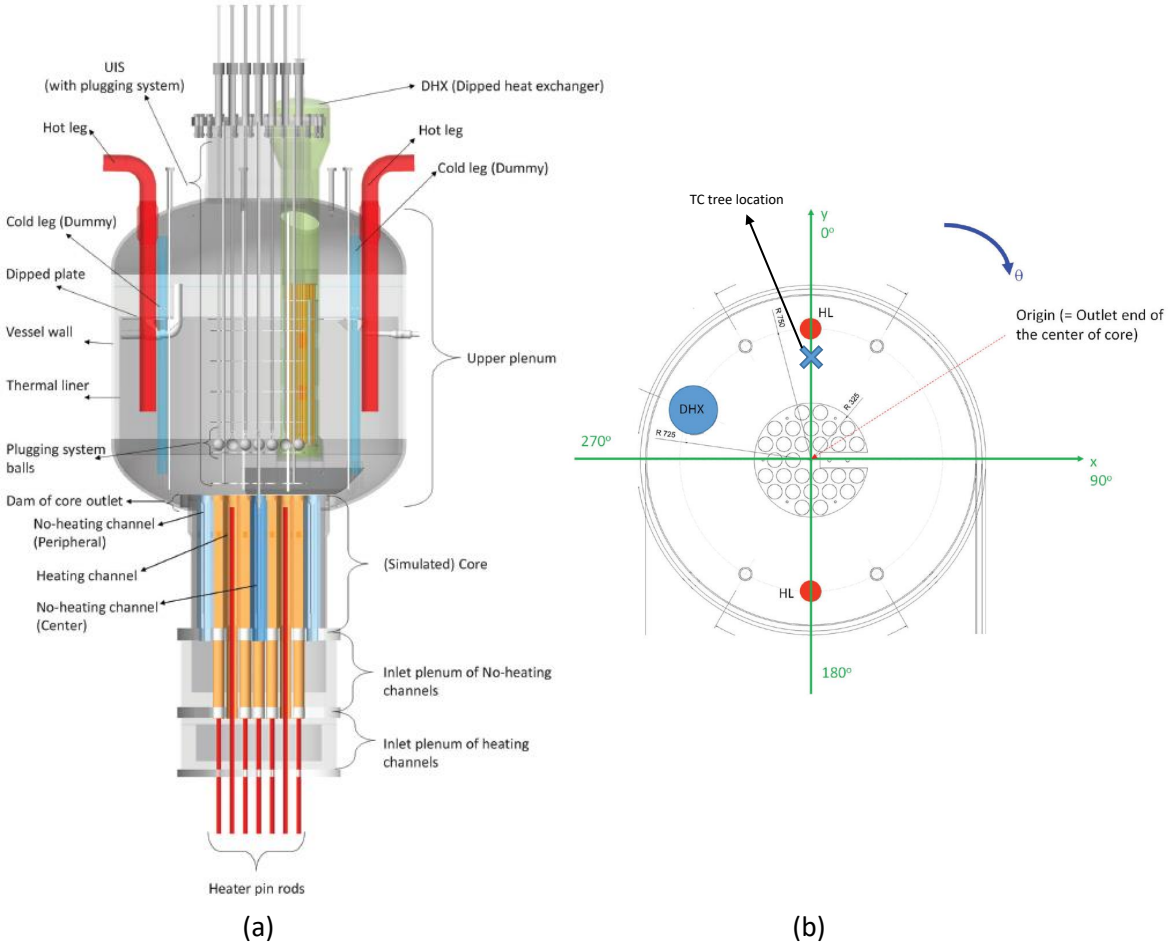

Figure 1. Overview of the PLANDTL-2 facility. (a) vertical cross view. (b) Horizontal cross-section seen from above. The coordinate system is defined in the right image.

primary circuit to the secondary circuit via the IHX and to the DHRS via the DHX. On the secondary side, a valve is used to impeach the circulation after a certain delay. Moreover, after a given delay that depends on the scenario, the DHRS takes over to cool the primary circuit, operating either in forced or natural circulation. Ultimate heat sinks are constituted of air coolers (AC). They are off in all scenarios for the secondary circuit, and are activated after a predetermined delay for the DHRS. The detailed transient scenarios are presented in Section 2.2.

2.2. Studied Transients

Eight scenarios are defined to study the transient response of the loop. They are detailed in Table I. Each test is labeled according to three letters X-Y-Z, each corresponding to different values taken by the parameter:

- X denotes the initial state of the primary circuit:
  - $X = C$ for cold. The initial primary flowrate is higher, $W = 800$ l/min before the transient start, thus, the temperature levels are lower and the primary circuit is cold;
  - $X = H$ for hot. The initial primary flowrate is fixed at $W = 400$ l/min prior to the transient start. The primary circuit is therefore hotter.
- Y describes the inertia of the secondary side closing dynamics.
  - $Y = I$ for high inertia, the closing time of the secondary circuit is fixed at $t = 1000$ s.

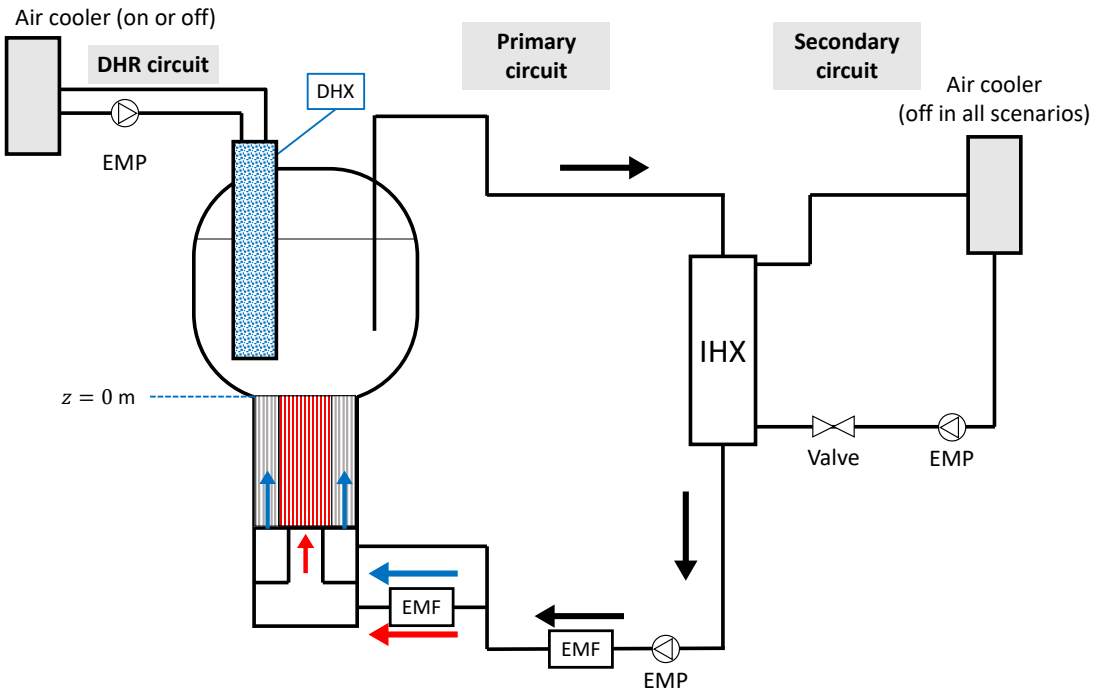

Figure 2. Simplified diagram in the considered transient scenarios. For clarity, the UIS is not shown and only one HL is displayed. Arrows indicate flow direction in normal operation.

  - $Y = L$ for low inertia, the closing time is fixed at $t = 100$ s.

- Z gives the operating mode of the DHR circuit.
  - $Z = F$ for forced circulation. The flowrate is imposed in the DHR circuit, and the AC power is imposed at 110 kW after 620 s.
  - $Z = N$ for natural circulation. The flow is let free. AC power is turned on after 9600 s (=160 min); except for case *C-L-N* where it is turned on after 620 s (= 10 min 20 s).

These eight scenarios permit to study in depth the effect of these parameters and their combinations. The obtained results will be then used as guidelines for future tests and concepts, as well as to provide a database for code validation.

3. EXPERIMENTAL RESULTS

In this section, the results are presented in three parts. We begin by examining the evolution of the transient flowrate and analyzing the influence of various parameters on the loop dynamics. Then, powers exchanged at each Heat EXchanger (HEX) are discussed. Finally, stratification evolution during the transients is discussed, and a link with primary flowrate stability is made.

3.1. Flow Circulation in Primary Circuit

In all studied cases, after the start of the transient, there is a quick decrease of the primary flowrate, due to turning off the primary pump. It decreases from 800 l/min (C cases) or 400 l/min (H cases) to values around 2.5 l/min, for all cases. We recall that the inlet of the core is fed by two separate lines. The heated

Table I. Transient conditions.

Test ID	Primary circuit		Secondary circuit			DHR circuit	
	Flowrate (l/min)	Core power (kW)	Flowrate (l/min)	Valve closing time (s)	A/C power (kW)	Flowrate (l/min)	A/C power (kW)
C-I-F	$800 \xrightarrow{10\,s} 0$	$500 \xrightarrow{10\,s} 0$	$250 \xrightarrow{5\,s} 0$	1000	$500 \xrightarrow{30\,s} 0$	90	$0 \xrightarrow{620\,s} 110$
C-L-F				100	$500 \xrightarrow{10\,s} 0$		$0 \xrightarrow{620\,s} 110$
H-I-F	$400 \xrightarrow{10\,s} 0$			1000	$500 \xrightarrow{30\,s} 0$		$0 \xrightarrow{620\,s} 110$
H-L-F				100	$500 \xrightarrow{10\,s} 0$		$0 \xrightarrow{620\,s} 110$
C-I-N	$800 \xrightarrow{10\,s} 0$			1000	$500 \xrightarrow{30\,s} 0$	$90 \xrightarrow{10\,s} 0$	$0 \xrightarrow{9600\,s} 110$
C-L-N				100	$500 \xrightarrow{10\,s} 0$		$0 \xrightarrow{620\,s} 110$
H-I-N	$400 \xrightarrow{10\,s} 0$			1000	$500 \xrightarrow{30\,s} 0$		$0 \xrightarrow{9600\,s} 110$
H-L-N				100	$500 \xrightarrow{10\,s} 0$		$0 \xrightarrow{9600\,s} 110$

channels (resp. unheated) are fed by the lower plenum (resp. upper plenum), as shown in Figure 2, with a volume flowrate W_{heat} (resp. W_{unheat}). Finally, we have:

$$W_I = W_{heat} + W_{unheat}. \tag{1}$$

First, at large time-scales, $t \gg 300$ min, it is observed that the primary flowrate is similar in all cases, around $W_I \approx 2.5$ l/min. However, the unheated channel flowrate is negative, $W_{unheat} \approx -0.2$ l/min. This shows that for all cases, in steady regime, the fluid rises through the heated channels. A significant amount of it flows towards the HL, while a smaller portion goes down around the core, through unheated channels. This fluid then mixes with the fluid coming from the HL, upstream of the line division (see Figure 2). The dynamics at intermediate times, $t \leq 300$ min, however depends on the scenario, as shown in Figure 3 for selected cases. It is seen that in forced cases, flow reversals $W_I \leq 0$ occur between 100 min $\leq t \leq 300$ min. As it will be discussed in Section 3.3, the origin of these reversals is linked with thermal stratification in the hot pool. The amplitude of the fluctuations can reach $W_I \pm 10$ l/min. Such variations might lead to thermal oscillations, thermomechanical fatigue and/or vibrations of the structures.

In the secondary side, the flowrate decreases abruptly at $t = 100$ s for L cases, and at $t = 1000$ s for I cases. In the DHR circuit, the flowrate W_{DHX} also quickly drops in the early stages of the transient for N cases. It then increases progressively due to heat exchange with the primary circuit and natural circulation on the DHR circuit side. An abrupt increase of W_{DHX} from $W_{DHX} \approx 20$ l/min to ≈ 30 l/min occurs at $t = 160$ min (or 9600 s), which corresponds to the activation of the AC on the DHR side. For F cases, the flowrate remains imposed constant $W_{DHX} = 90$ l/min.

3.2. Heat Exchangers Performance

The power at each HEX is computed as follow, and is shown in Figure 8. For the IHX, temperature measurements are available on both the primary and the secondary sides. The power received by the IHX secondary side is directly:

$$\dot{Q}_{IHX} = \rho W_{II} c_p \Delta T_{IHX,II}\ , \tag{2}$$

with $\Delta T_{IHX,II}$ the temperature difference at the IHX on the secondary side, W_{II} the volume flowrate of the secondary circuit, and ρ the sodium volumetric mass. Neglecting heat losses at the IHX, the exchanged power as defined in Equation (2) is equivalent to the power extracted from the primary circuit at the IHX:

$$\dot{Q}_{IHX} = \rho W_I c_p \Delta T_{IHX,I}\ , \tag{3}$$

with $\Delta T_{IHX,I}$ the temperature difference at the IHX on the primary side. These two definitions are equivalent in steady-state for an adiabatic HEX. As seen here, there is a difference, which highlights

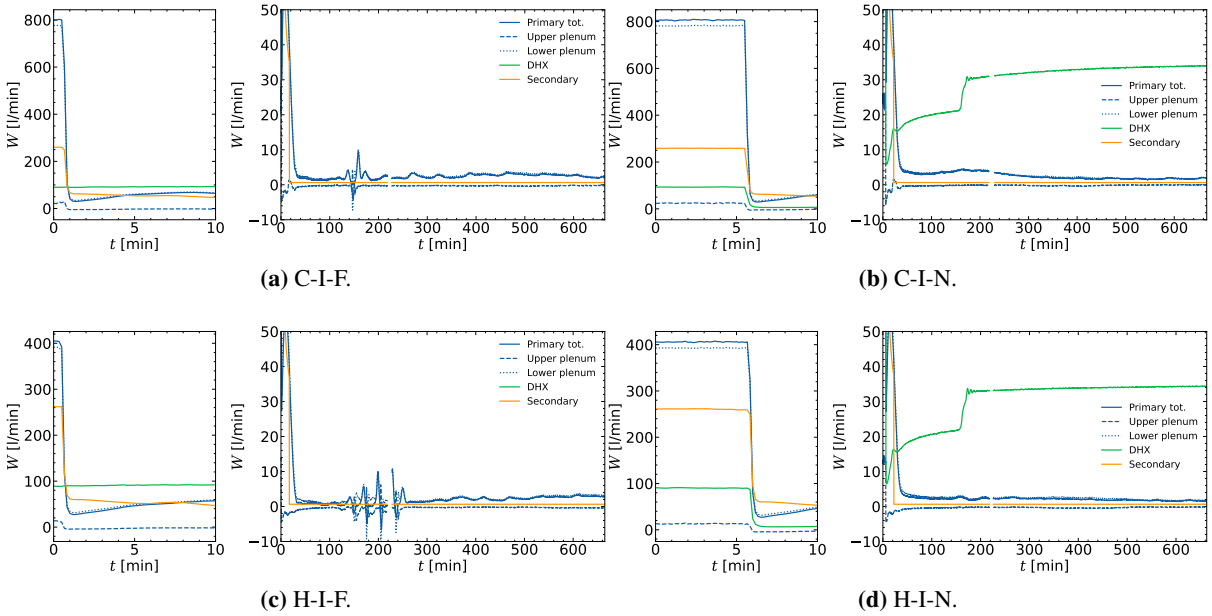

(a) C-I-F. **(b)** C-I-N.

(c) H-I-F. **(d)** H-I-N.

Figure 3. Flowrate evolution in each component for selected cases. The left panel shows the flowrate in the early stage of the transient. The right panel focuses on a reduced vertical scale to highlight the flowrates in the intermediate stages.

heat losses at the IHX. For the DHX, the exchanged power is given by:

$$\dot{Q}_{DHX} = \rho W_{DHX} c_p \Delta T_{DHX} \ , \tag{4}$$

where ΔT_{DHX} is measured in the DHR side. In all cases, the electrical power is fixed at $\dot{Q}_{elec} = 110$ kW. The heat balance on the primary circuit then gives:

$$\dot{Q}_I = \dot{Q}_{st} + \dot{Q}_{loss} = \dot{Q}_{elec} - \dot{Q}_{IHX} - \dot{Q}_{DHX}. \tag{5}$$

Here $\dot{Q}_I$ represents the combined heat stored in the primary circuit $\dot{Q}_{st}$ and the heat losses $\dot{Q}_{loss}$. It is not possible to distinguish between $\dot{Q}_{st}$ and $\dot{Q}_{loss}$ in this context. Therefore, $\dot{Q}_I$ is deduced from the measurement of powers at the core, the IHX and the DHX. As indicated by the sign convention in Equation (5), all quantities are treated as positive.

Despite variations in flowrates and flow reversals, the various exchanged powers exhibit smoother behavior. As shown in Figure 4, the large amplitude oscillations observed on the flowrate are not reflected in the powers transferred at the HEXs. First, in F cases, $\dot{Q}_{DHX}$ rises quickly to compensate $\dot{Q}_{elec}$, and we have after a few minutes $\dot{Q}_{DHX} \approx \dot{Q}_{elec}$. The difference is likely due to heat losses. During the initial moments of the transients, the net stored power in the primary circuit becomes negative, highlighting an initial global cooling of the system.

On the other hand, for N cases, the stored power increases to $\dot{Q}_{st} \approx 100$ kW and slowly decays. It is compensated by the action of the DHR circuit, as $\dot{Q}_{DHX}$ gradually increases in the same fashion as $\dot{Q}_{DHX}$ decreases. Similarly, as for the flowrate, the activation of AC at $t = 160$ min has a drastic effect on $\dot{Q}_{DHX}$, which abruptly increases from $\dot{Q}_{DHX} \approx 25$ kW to a value between 60 and 75 kW, depending on the cases. An abrupt decrease of $\dot{Q}_{st}$ is simultaneously observed. After the AC activation, $\dot{Q}_{DHX}$ slowly increases towards $\dot{Q}_{elec}$. It is noticeable that the increase is quicker for H cases. This is explained by the fact that in H cases, the temperature difference between the primary side and the DHR circuit side is larger, thus the heat flux is larger.

For all cases, $\dot{Q}_{IHX}$ falls to values much smaller than $\dot{Q}_{DHX}$, but the heat transfer at the IHX is not necessarily zero. Notably, the temperatures evolution at the IHX depends on N or F cases, as shown in Figure 5. For F cases, the inlet temperature on primary side $T_{in,IHX,I}$ decreases quickly. Indeed, the heat

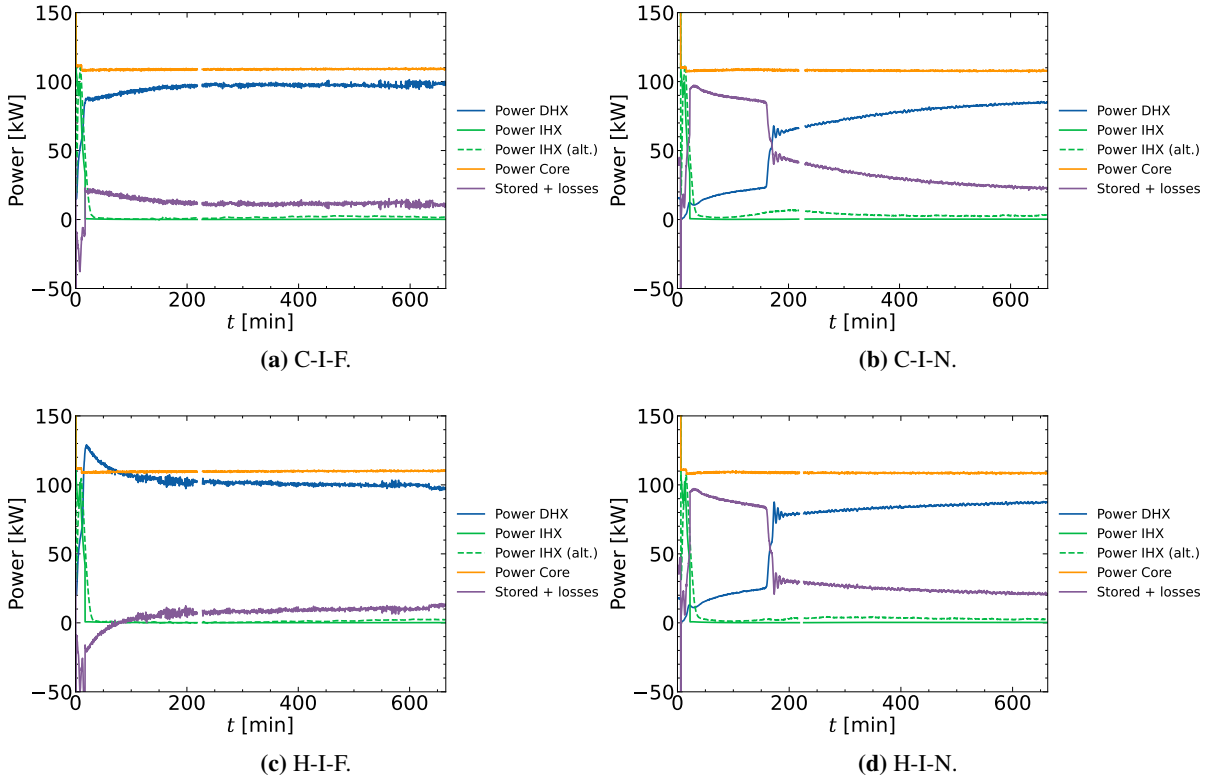

(a) C-I-F. **(b)** C-I-N.

(c) H-I-F. **(d)** H-I-N.

Figure 4. Heat transfer evolution in each component for selected cases.

is removed rapidly from the plenum, due to forced circulation in the DHR circuit, and the temperature drops. On the opposite, the secondary side is closed, therefore there is no more heat transfer at the IHX, and $T_{out,IHX,I}$ increases. The abrupt decrease of $T_{in,IHX,I}$ eventually leads to a pinching of the inlet and outlet temperatures $T_{in,IHX,I} \approx T_{out,IHX,I}$, and the heat transfer at the IHX is annihilated. As it will be discussed in Section 3.3, this phenomenon is of importance for the loop stability. Indeed, it is observed that the pinching occurs simultaneously with the flow reversals (Figure 3).

3.3. Evolution of Stratification and Stability

The temporal evolution of temperature profiles near the inlet of one HL is shown in Figure 6 for all transients. The profiles are taken from a TC-tree located at coordinates $x = 0$ mm, $y = 590$ mm, and indicated in Figure 1b. Several observations can be made. First, for N cases, the average temperature of a given height increases gradually over the course of the transient, with a weak thermal stratification. For H-I-N and H-L-N cases, the temperature is initially close to 360°C and increases to 440-450°C. For C-I-N and C-L-N cases, the initial average temperature is close to 340°C and rises up to 400-420°C. Hence, the initial temperature level (C or H) plays on the final temperature, but weakly affects how temperatures rise in the pool. Different conclusions are drawn for F cases, due to the higher extracted thermal power through the DHX. Here, the initial average temperature is around 330°C for C-I-F and C-L-F cases, and around 360°C for H-I-F and H-L-F cases. The transient evolution of temperature profiles is dependent on the initial condition for F cases. Indeed, in C-I-F and C-L-F cases, the pool temperature rises towards the steady-state value, close to 340°C in the upper part. On the other hand, in H-I-F and H-L-F cases, the temperature profiles decrease until they reach values close to 360°C in the upper part of the pool. Moreover, in all cases, an increase of thermal stratification is noticed.

This latter phenomenon is observed more easily thanks to the temperature gradient profiles, as shown in Figure 7. At the start of the transient, the stratification is weak for all considered cases, with $dT/dz \approx$ 20°C/m near the bottom of the pool. However, for F cases, the thermal stratification quickly increases

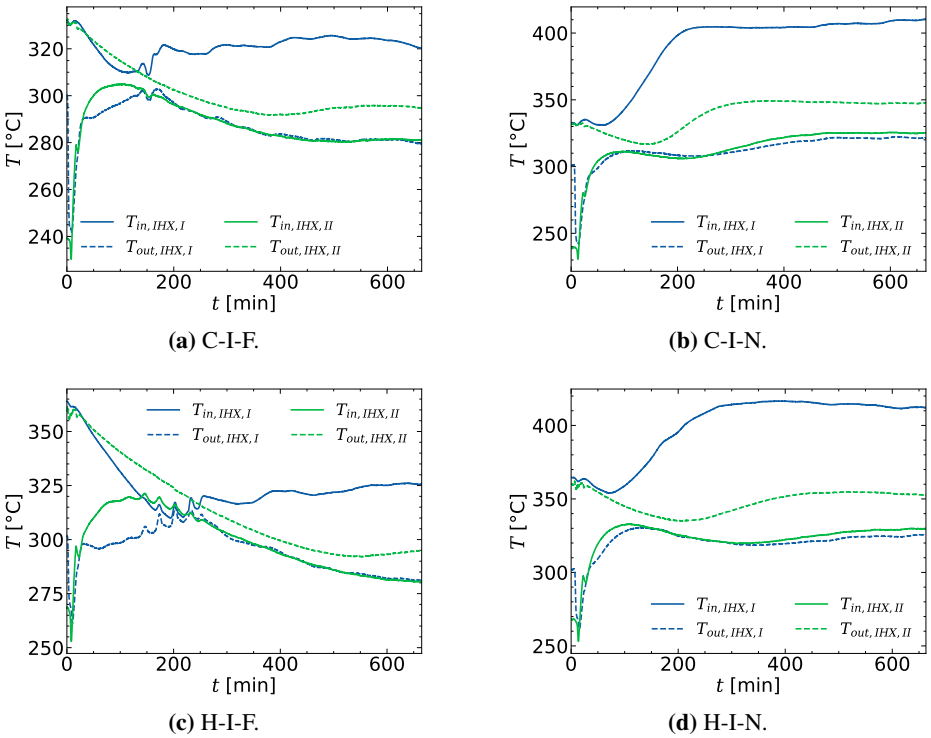

(a) C-I-F. **(b)** C-I-N. **(c)** H-I-F. **(d)** H-I-N.

Figure 5. Temperatures at the inlets and outlets of the IHX.

to values close to $dT/dz \approx 60$°C/m near the bottom of the hot pool. The final stratification profile is reached for all F cases in less than 45 minutes. A different behavior is observed for N cases. Indeed, during the early phases of the transients, the stratification does not evolve strongly, and remains close to $dT/dz \approx 20$°C/m near the bottom. A sudden change occurs as the DHRS AC is turned on, at $t = 160$ min. The thermal stratification then reaches similar values to F cases, with $dT/dz \approx 60$°C/m at the bottom of the pool. The only exceptions are for C-L-N case, where the DHX AC is turned earlier, at 620 s, similarly to F cases. Here, the stratification progressively increases from 20°C/m to 60°C/m, but over a time span of 600 min, contrary to F cases where the increase occurs in around 10 minutes. This highlights that the increase in stratification is due to the heat extraction at the DHX. It is increased when the DHR circuit AC is activated (increase of $\dot{Q}_{DHX}$), and further increased due to the imposed flow on the DHR side (strong increase of $\dot{Q}_{DHX}$). It is also noticeable that the upper part of the hot pool, $z \geq 600$ mm, is weakly stratified in all cases. As discussed in Section 4, this stratification intensification plays a key role on the loop stability. Indeed, as shown in Figures 6 and 7, the HL inlet is located around $z \approx 400$ mm.

4. DISCUSSION AND DESIGN GUIDELINES

The results presented here show an increase in stratification when the DHRS operates in forced circulation. This is due to an increase of heat extraction that leads to a quick cooling of the pool. In turn, the fluid entering the HLs is cold, and a temperature pinching occurs at the IHX. In consequence, the driving term becomes zero and natural circulation through the primary circuit is annihilated. The power extracted at the IHX and DHX are shown in Figure 8. The N cases are shown in blue, while the F cases are shown in black. The C-L-F case is highlighted in green, as it is the only F case that does not display flow reversals. Globally, it is observed that all F cases have a higher $\dot{Q}_{DHX}$ and a lower $\dot{Q}_{IHX}$. However, it not sufficient to determine a stability threshold, due to the case C-L-F. The instability presented here results from the competition between the heat removal by circulation through the primary circuit, versus the stratification increase induced by the DHRS.

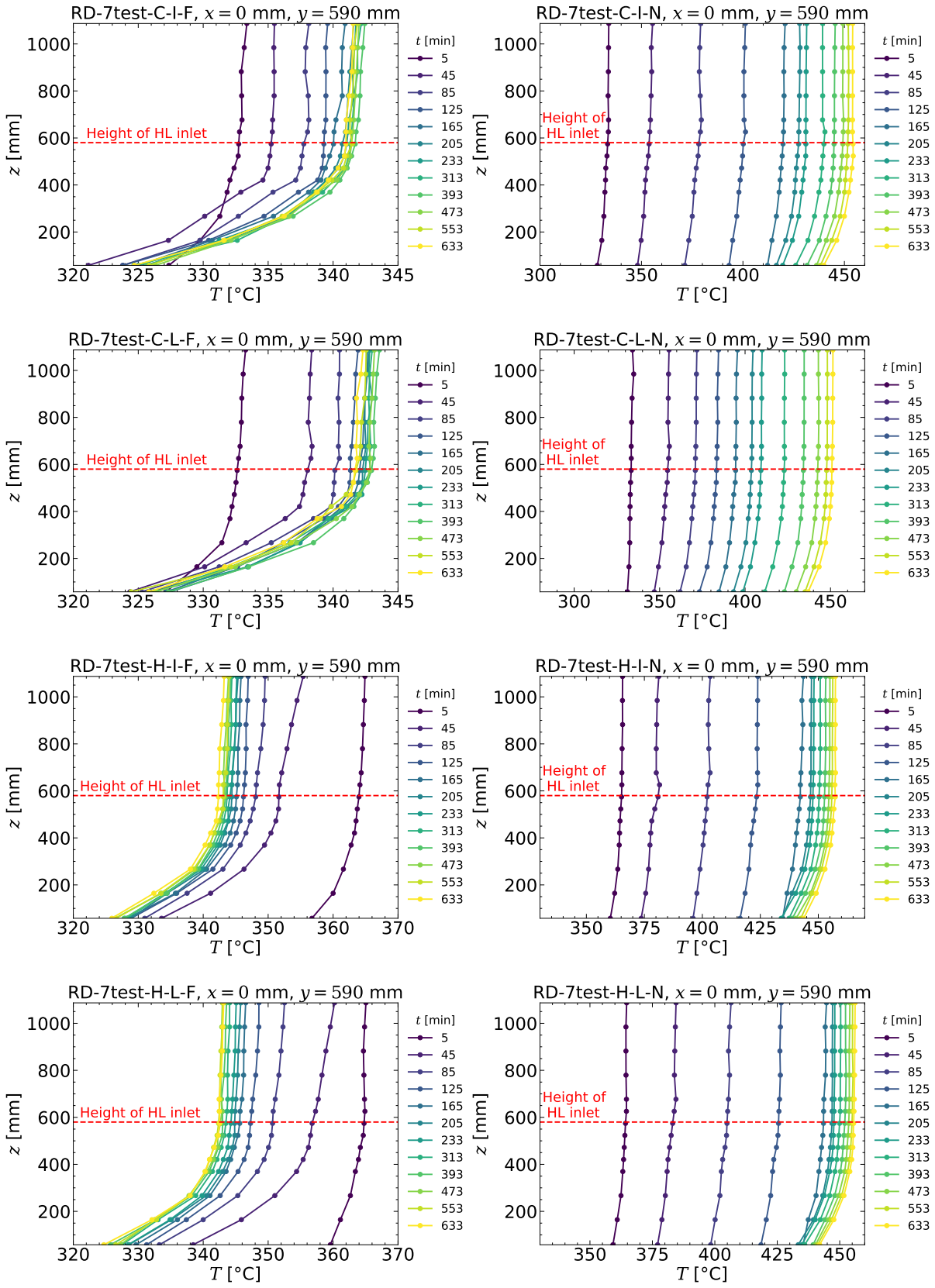

Figure 6. Temperature profiles during the transients.

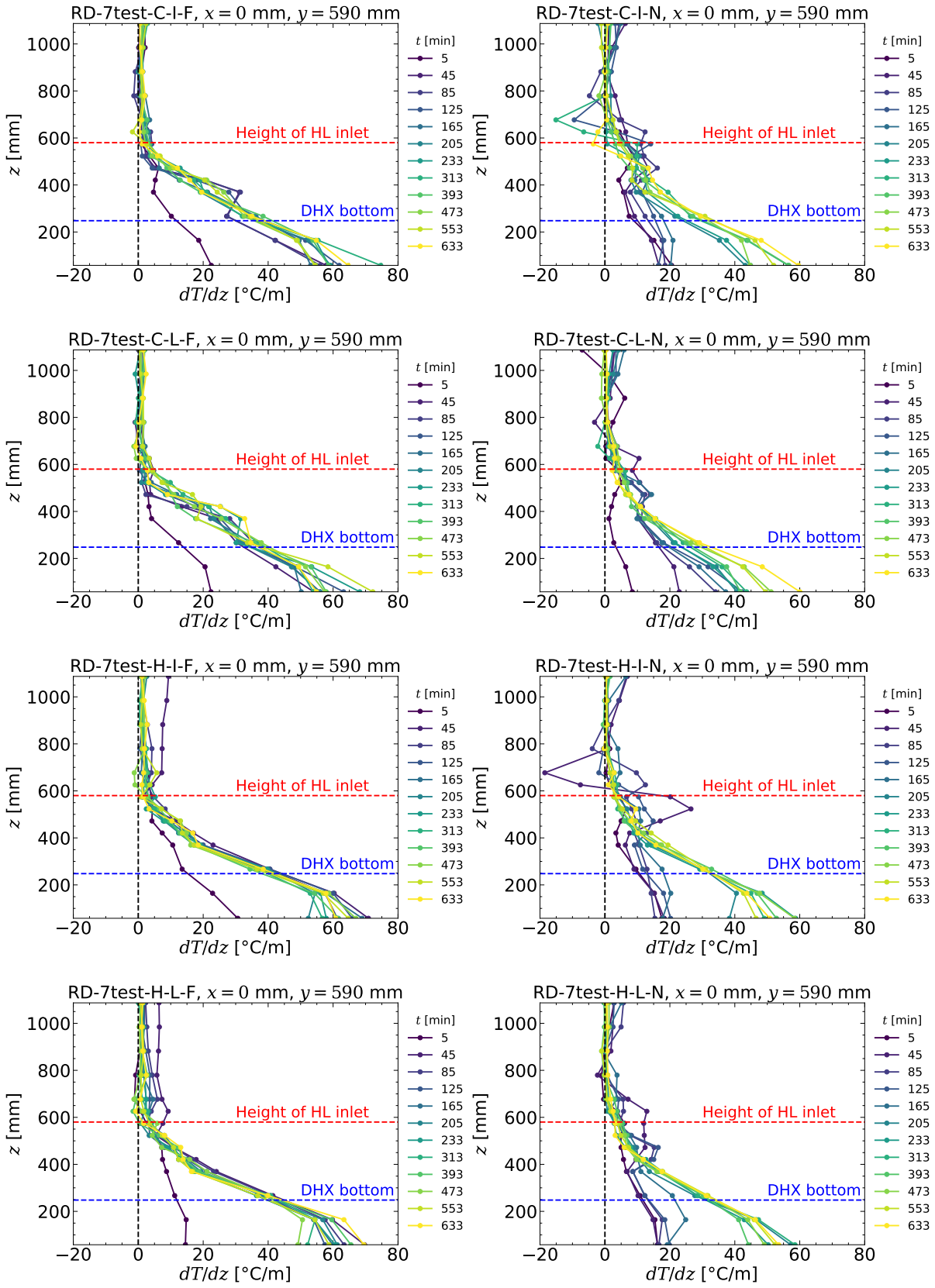

Figure 7. Evolution of stratification over time for all cases.

To compare these effects, the Stanton number of the system is here defined as:

$$St = \frac{\text{Heat removal at DHX}}{\text{Convection through primary circuit}} = \frac{Nu_{DHX}}{Re_I\, Pr} \tag{6}$$

where the Nusselt, Reynolds, and Prandtl numbers are respectively defined as:

$$Nu = \frac{h_{DHX} H_{DHX}}{\lambda}\,, \quad Re_I = \frac{\rho D_I W_I}{A_I \mu}\,, \quad Pr = \frac{\mu}{\rho \kappa}. \tag{7}$$

Here, h_{DHX} is the heat transfer coefficient at the DHX, H_{DHX} is the effective exchange height of the DHX, λ is the sodium thermal conductivity, D_I is the primary circuit pipe diameter, $A_I = \pi D_I^2/4$ is the primary circuit pipe cross-sectional area, μ is the sodium dynamic viscosity, and $\kappa = \lambda/\rho c_p$ is the sodium thermal diffusivity.

It is well established in natural convection loops that St plays a key role in the stable or unstable loop behavior [16, 20]. Rigorously speaking, St should be defined using steady-state quantities. It is considered here that the system evolves slowly, in a quasi-static manner. The evolution of St is shown in Figure 9. The N cases all display the same temporal evolution, with slowly increasing St values. For F cases, St rises shortly after the transient beginning, and oscillates around values that depend on the scenario. It is observed that before the onset of instabilities, N cases are all well below $St \approx 20$, and F cases are all at $St \geq 20$, with the C-L-F case at $St \approx 20$. At the onset of flowrate oscillations, St also strongly oscillates. For all F cases, St values slowly decrease after the end of the oscillations, towards values similar to those of N cases. Consequently, $St \approx 20$ serves as a threshold for the onset of flow reversal in the investigated conditions. It is also clear that this value shall depend on the electrical power $\dot{Q}_{elec}$, but this parameter is not investigated here.

As the experimental conditions of PLANDTL-2 are representative of actual reactor concepts, some guidelines for future investigations can be given:

- The flow reversals originates in the stratified layer, near the bottom of the hot pool. Consequently, colder fluid enters the HL and annihilates circulation in the primary circuit. One could avoid reversals by putting the inlet of the HL at a higher elevation.
- Conversely, it could be interesting to evaluate the DHX elevation effect on stratification. A higher elevation might reduce the stratification increase.
- The flow reversals appear due to the strong and rapid increase of stratification. Delaying the activation of the DHRS AC could potentially avoid the reversals.

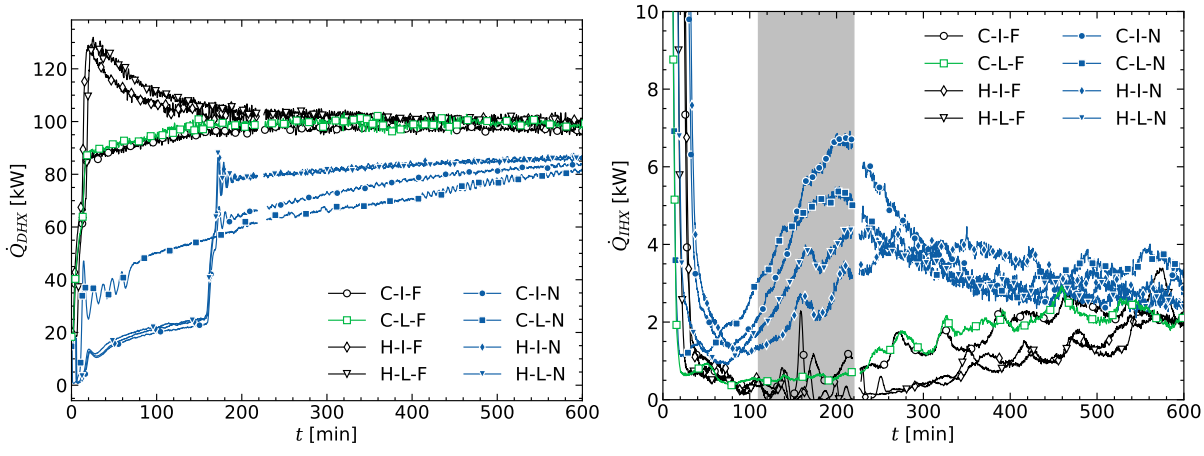

Figure 8. Power evolution at DHX and IHX.

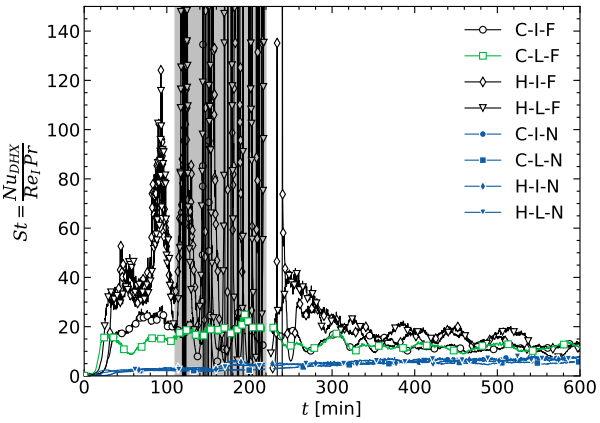

Figure 9. Stanton number evolution for all cases.

5. CONCLUSIONS AND PERSPECTIVES

In this paper, flowrate instabilities in natural circulation conditions in the IET named PLANDTL-2 were investigated. The loop behavior is determined by the competition between the circulation in the primary circuit and heat removal at the IHX, versus the heat removal at the DHRS. Eight scenarios were investigated, focusing especially on the operating mode of the DHRS (forced or free; with and without AC assist), the secondary side inertia (low or high), and the initial primary flowrate (low or high). First, it was observed that the initial conditions and initial phases ($<$ 10 min approximately) had a weak influence on the long term behavior. All cases converge to a steady-state (after $\sim$600 min) that mainly depends on the operating mode of the DHRS. The temperature levels in the hot pool are around $\sim$340°C in forced circulation (F) cases, and around 440°C in natural circulation (N) cases. On the one hand for F cases, the forced operation and AC of the DHRS is imposed shortly after the beginning of the transient, when natural circulation is not yet established. As a consequence, strong stratification is induced and perturbs the circulation establishment due to loss of buoyancy driving term at the IHX. On the other hand, for N cases, the DHRS AC is activated later, when the circulation is already established. In these cases, a jump in heat transfer at the DHX and the stratification enhancement are still observed, but do not modify the circulation throughout the primary circuit. The analysis of the physical mechanism lead to determining a non-dimensional criteria based on the Stanton number to predict the flow stability.

The results presented are counterintuitive, as the objective is typically to cool the core rapidly. However, this study demonstrates that excessively rapid or early cooling can result in instabilities and flow reversals. Furthermore, it is observed that the stratification mechanism, a three-dimensional effect, plays a critical role. These effects are typically not captured in system-scale models, necessitating the implementation of strategies to account for them. Examples include multiscale simulations [9] or alternative one-dimensional modeling approaches [7].

The collected data will serve as a validation database for multiscale calculation tools. Additionally, an in-depth study of core cooling facilitated by the IWF is of interest. Investigating other experimental transients, such as shutting off the AC after an extended period, would also be valuable. Such experiments could provide insights into the persistence or dissipation of thermal stratification in the hot pool. Also, geometrical modifications of the loop could be of interest to evaluate the effect of the DHX position, HLs inlet or the UIS.

ACKNOWLEDGMENTS

This study is carried out in the framework of the France/Japan collaboration agreement on Sodium Fast Reactors. S. Renaudière de Vaux and S. Li acknowledge fruitful discussions with Antoine Gerschenfeld and Yannick Gorsse.

NOMENCLATURE

Abbreviations and acronyms

AC	Air Cooler (ultimate heat sink)
CFD	Computational Fluid Dynamics
CL, HL	Cold Leg, Hot Leg
DHRS	Decay Heat Removal System
DHX	Dipped Heat eXchanger
EMF	ElectroMagnetic Flowmeter
EMP	ElectroMagnetic Pump
HEX	Heat EXchanger
IET	Integral Effect Test
IHX	Intermediate Heat eXchanger
IWF	Inter Wrapper Flow
MAE	Mean Absolute Error
PLANDTL-2	Plant Dynamics Test Loop 2
SET	Separate Effect Test
UIS	Upper Internal Structure

Greek letters

κ	Thermal diffusivity, [m^2/s]
λ	Thermal conductivity, [W/m.K]
μ	Dynamic viscosity, [Pa.s]
ρ	Density, [kg/m^3]

Latin letters

$\dot{Q}$	Power, [W]
c_p	Heat capacity, [J/K]
H	Height, [m]
h	Heat transfer coefficient, [W/m^2.K]
T	Temperature, [°C]
W	Volume flowrate, [m^3/s] or [l/min]

Nondimensional numbers

Nu	Nusselt number, hH/λ
Pr	Prandtl number, $\mu/\rho\kappa$
Re	Reynolds number
St	Stanton number, $Nu/(RePr)$

Subscripts

DHX, IHX	relative to the DHX, the IHX
$heat$, $unheat$	relative to the heated and unheated channels
I, II	relative to primary, secondary circuit
in	inlet
out	outlet

References

[1] U Parthasarathy, T Sundararajan, C Balaji, K Velusamy, P Chellapandi, and SC Chetal. Decay heat removal in pool type fast reactor using passive systems. *Nuclear engineering and design*, 250:480–499, 2012.

[2] G Vaidyanathan. Decay heat removal in sodium cooled fast reactors-an overview. *Annals of Nuclear Energy*, 205:110554, 2024.

[3] F Roelofs, A Gerschenfeld, M Tarantino, K Van Tichelen, and WD Pointer. Thermal-hydraulic challenges in liquid-metal-cooled reactors. In *Thermal Hydraulics aspects of liquid metal cooled nuclear reactors*, pages 17–43. Elsevier, 2019.

[4] Muhammad Younas Ali, Guowei Wu, Shuyong Liu, Ming Jin, Zhumin Zhao, and Yican Wu. CFD analysis of thermal stratification under PLOFA transient in CLEAR-S. *Progress in Nuclear Energy*, 115:21–29, 2019.

[5] Dmitry Grishchenko, A Papukchiev, C Liu, C Geffray, M Polidori, K Kööp, Marti Jeltsov, and Pavel Kudinov. TALL-3D open and blind benchmark on natural circulation instability. *Nuclear Engineering and Design*, 358:110386, 2020.

[6] David Pialla, Denis Tenchine, Simon Li, Paul Gauthe, Alfredo Vasile, Roland Baviere, Nicolas Tauveron, Fabien Perdu, Ludovic Maas, François Cocheme, et al. Overview of the system alone and system/CFD coupled calculations of the PHENIX Natural Circulation Test within the THINS project. *Nuclear Engineering and Design*, 290:78–86, 2015.

[7] Zeyun Wu, Cihang Lu, Sarah Morgan, Sama Bilbao y Leon, and Matthew Bucknor. A status review on the thermal stratification modeling methods for sodium-cooled fast reactors. *Progress in Nuclear Energy*, 125:103369, 2020.

[8] Yapeng Liu, Dalin Zhang, Lei Zhou, Kailong Chen, Wenxi Tian, Suizheng Qiu, and GH Su. Analysis of the effect of thermal stratification on the natural circulation decay heat removal of sodium-cooled fast reactor. *Progress in Nuclear Energy*, 167:104979, 2024.

[9] G Bandini, M Polidori, A Gerschenfeld, D Pialla, S Li, WM Ma, Pavel Kudinov, Marti Jeltsov, Kaspar Kööp, K Huber, et al. Assessment of systems codes and their coupling with cfd codes in thermal–hydraulic applications to innovative reactors. *Nuclear Engineering and Design*, 281:22–38, 2015.

[10] M Azarian, M Astegiano, M Tenchine, M Lacroix, and M Vidard. Sodium thermal-hydraulics in the pool LMFBR primary vessel. *Nuclear engineering and design*, 124(3):417–430, 1990.

[11] Jung Yoon, Jewhan Lee, Hyungmo Kim, Yong-Bum Lee, and Jaehyuk Eoh. Heat transfer characteristics of redan structure in large-scale test facility STELLA-2. *Nuclear Engineering and Technology*, 53(4):1109–1118, 2021.

[12] Jewhan Lee, Jaehyuk Eoh, Jung Yoon, Seok-Kwon Son, and Hyungmo Kim. Heat transfer system design of sodium test facility STELLA-2. *Annals of Nuclear Energy*, 191:109930, 2023.

[13] M Nishimura, H Kamide, K Hayashi, and K Momoi. Transient experiments on fast reactor core thermal-hydraulics and its numerical analysis: Inter-subassembly heat transfer and inter-wrapper flow under natural circulation conditions. *Nuclear engineering and design*, 200(1-2):157–175, 2000.

[14] JA Boure, AE Bergles, and L S_ Tong. Review of two-phase flow instability. *Nuclear engineering and design*, 25(2):165–192, 1973.

[15] Leonardo Carlos Ruspini, Christian Pablo Marcel, and Alejandro Clausse. Two-phase flow instabilities: A review. *International journal of heat and mass transfer*, 71:521–548, 2014.

[16] Pallippattu Krishnan Vijayan, Arun K Nayak, and Naveen Kumar. *Single-phase, two-phase and supercritical natural circulation systems*. Woodhead Publishing, 2019.

[17] M Misale. Experimental study on the influence of power steps on the thermohydraulic behavior of a natural circulation loop. *International Journal of Heat and Mass Transfer*, 99:782–791, 2016.

[18] Ayako Ono, Masaaki Tanaka, Yasuhiro Miyake, Erina Hamase, and Toshiki Ezure. Preliminary analysis of sodium experimental apparatus PLANDTL-2 for development of evaluation method for thermal-hydraulics in reactor vessel of sodium fast reactor under decay heat removal system operation condition. *Mechanical Engineering Journal*, 7(3):19–00546, 2020.

[19] Hideki Kamide, Tai Asayama, Takashi Wakai, Toshiki Ezure, Akihiro Uchibori, Shigenobu Kubo, and Masayuki Takeuchi. Progress of sodium-cooled fast reactor developments in Japan taking into account total lifecycle, risk-informed approach, and sustainability. *Nuclear Engineering and Design*, 421:113062, 2024.

[20] PK Vijayan, M Sharma, and D Saha. Steady state and stability characteristics of single-phase natural circulation in a rectangular loop with different heater and cooler orientations. *Experimental Thermal and Fluid Science*, 31(8):925–945, 2007.

[21] E Hourcade, T Mihara, A Dauphin, A Ide, and J-F Dirat. Astrid nuclear island design update in french-japanese joint team development of decay heat removal systems. In *2018 International Congress on Advances in Nuclear Power Plants (ICAPP 18)*, 2018.